

Article

The Tribological Properties of Plasma Electrolytic Oxidation Layers Synthesized on Arc Spray Coatings on Aluminum Alloys in Contact with Various Friction Materials

Volodymyr Hvozdet's'kyi ¹, Juozas Padgurskas ^{2,*} , Mykhailo Student ^{1,*}, Iryna Pohrelyuk ¹, Oleksandra Student ¹, Khrystyna Zadorozhna ¹, Oleh Tkachuk ¹ and Raimundas Rukuiza ^{2,*} 

¹ Karpenko Physico-Mechanical Institute of the National Academy of Sciences of Ukraine, 5, Naukova Str., 79060 Lviv, Ukraine; gvosdetcky@nas.gov.ua (V.H.); pohrelyuk@nas.gov.ua (I.P.); o.student@nas.gov.ua (O.S.); kh-zadorozhna@nas.gov.ua (K.Z.); o-tkachuk@nas.gov.ua (O.T.)

² Department of Mechanical, Energy and Biotechnology Engineering, Vytautas Magnus University, LT-53361 Kauno r, Lithuania

* Correspondence: juozas.padgurskas@vdu.lt (J.P.); student@nas.gov.ua (M.S.); raimundas.rukuiza@vdu.lt (R.R.)

Abstract: Oxide layers on the surface of the aluminum alloys D16 and AMg6 and on arc coatings sprayed with electrode wires made of the alloys D16 and AMg6 were synthesized using plasma electrolytic oxidation (PEO). The microstructure, phase composition and micro-hardness of the PEO layers were studied. In addition to the two main phases (α -Al₂O₃ and γ -Al₂O₃), a small amount of a metastable crystalized Al_{2.427}O_{3.64} phase was found in their structure. A comparison was made of the wear resistance and friction coefficients of the synthesized PEO layers during friction tests in pairs with other PEO layers, a galvanic chromium coating, cast iron, steels and bronze of the BrC30 type. The results of the friction tests for the various PEO layers on aluminum alloys in tribo-contact with high-hardness elements made of hardened or chrome-plated steel justify the possibility of their use in a friction pair. We experimentally showed the influence of glycerin additive in motor oil 15W30 on the change in the friction coefficient of the PEO layers synthesized on the aluminum alloys and on the arc-sprayed coatings on their surfaces in tribocouples with hardened steel.

Keywords: arc-sprayed coatings; plasma electrolytic oxide layers; tribological characteristics



Citation: Hvozdet's'kyi, V.; Padgurskas, J.; Student, M.; Pohrelyuk, I.; Student, O.; Zadorozhna, K.; Tkachuk, O.; Rukuiza, R. The Tribological Properties of Plasma Electrolytic Oxidation Layers Synthesized on Arc Spray Coatings on Aluminum Alloys in Contact with Various Friction Materials. *Coatings* **2024**, *14*, 460. <https://doi.org/10.3390/coatings14040460>

Academic Editors: Huirong Le and Esteban Broitman

Received: 25 February 2024

Revised: 23 March 2024

Accepted: 5 April 2024

Published: 10 April 2024



Copyright: © 2024 by the authors. Licensee MDPI, Basel, Switzerland. This article is an open access article distributed under the terms and conditions of the Creative Commons Attribution (CC BY) license (<https://creativecommons.org/licenses/by/4.0/>).

1. Introduction

In many cases, the main reason for the premature failure of machine parts, mechanisms and metal elements in engineering structures is damage to their surface due to corrosion, erosion, cavitation or mechanical wear of their working surfaces, often enhanced by the influence of the technological environment in which they are operated [1–7].

To increase the wear resistance of light alloys, as well as their anti-corrosion protection, the following technological methods are currently used:

- Galvanic chrome, nickel, zinc or alloy plating, as well as the creation of composite coatings [8–12],
- Vacuum deposition of coatings [13–15],
- Laser melting of the surface layers with the incorporation of dispersed carbide particles into the molten layers [16–20],
- The thermal spray coating method [21–28].

All these technological approaches are widely used to protect and restore the dimensions of worn parts.

Plasma electrolytic oxidation (PEO) is a relatively new type of treatment for hardening the surface of metallic materials. Its use makes it possible to obtain multifunctional layers (similar to ceramics) with a unique set of properties. PEO layers have high wear resistance, corrosion resistance and heat resistance, as well as electrical insulating and decorative

properties [29–34]. Depending on the chemical composition of the aluminum alloys, PEO layers with different contents of α , γ , δ and η phases are formed on their surface. The ratio of these phases in the PEO layers determines their functional properties. In particular, the content of the α phase in these layers determines their hardness and wear resistance [35–37]. The specific content of certain phases depends on the chemical composition of the alloys and the parameters of the PEO process [38–41].

The expansion of the functionality of thermally sprayed aluminum coatings after their modification using PEO processing has already been demonstrated previously [42–48]. For the same purpose, plasma or cold spray deposition of aluminum coatings is also used [49,50], and aluminum, steel and titanium are used as the substrates [51–58].

PEO treatment of thermally sprayed aluminum alloy coatings on substrates of aluminum, magnesium and titanium alloys allows for the formation of oxide ceramic layers on their surface [59–64]. Their properties correspond to those of the PEO layers synthesized on the aluminum alloys. The features and mechanisms of the formation of PEO layers on phase-inhomogeneous substrates, in particular, composite materials based on aluminum and other metals, have also been reported [65].

The highest hardness (1460 HV_{0.1}, max. 1600 HV_{0.1}) has been obtained in PEO layers synthesized on an AlCu₄Mg₁ coating, which was formed using arc spraying. Its hardness was 55% higher than an aluminum oxide coating formed using plasma spraying in the atmosphere (940 HV_{0.1}). X-ray diffraction analysis showed that, as a rule, the lower hardness of the PEO layer on an aluminum alloy deposited using cold spraying is due to its lower content of α -Al₂O₃ [42]. A technological layer forms on the outer surface of the PEO layer, which has fairly high mechanical properties under wear conditions and provides good protection against corrosion. Meanwhile, its dense internal (functional) layer has better corrosion characteristics [66–69].

However, there is still no complete understanding of the features that arise during the frictional interaction of PEO layers paired with counter bodies made of different materials. Understanding the patterns of the changes in the tribological characteristics of various friction systems is important both for their practical use and for studying the nature of the phenomena accompanying the friction process. Therefore, the purpose of the study was to study the functional properties (wear resistance, friction coefficients) of synthesized PEO layers on two aluminum alloys (AMg16 and D16) during their tribo-contact with other PEO layers, electroplated with chromium, cast iron, steel and BrC30 bronze. In addition, since the friction process significantly depends on the presence of lubricant in the contact zone, it is also important to analyze the possibility of reducing the friction coefficient using lubricant additives.

The research design involves consideration of the following sequence of wear features in various friction pairs, which is relevant both to practice and to understanding the nature of the processes responsible for wear. The methodological part briefly describes the features of the applied methods for hardening the surface layers of aluminum alloys and certifying their capabilities when working in friction pairs. Then, the structure and phase composition of the plasma electrolyte oxidation layers synthesized on the surface of arc spray coatings (ASCs) obtained in the supersonic spraying mode using electrodes made of the high-strength aluminum alloys FMG6 and D16 were analyzed. The following also presents the results on the friction coefficients, tribocontact temperature and wear values for various friction pairs (both direct and reverse friction pairs) when one or both of their elements contain a PEO layer synthesized on the surface of an ASC deposited in the supersonic spraying mode using electrodes made of D16 alloys. Next, the possibility of additionally increasing the wear resistance characteristics of the PEO layers on the ASC by adding a small amount of glycerin to the working lubricant was analyzed, and results were presented that suggested the implementation of mass transfer between the elements of the friction pairs. Finally, conclusions based on the research results are formulated.

2. Materials and Methods

The arc spray coatings were formed by spraying AMg6, D16 and A0 wires (their chemical composition is shown in Table 1) onto a D16 alloy substrate using an electric arc metallizer developed at Karpenko Physico-Mechanical Institute of the National Academy of Sciences of Ukraine (Figure 1). Their use made it possible to form ASCs with high adhesion and low porosity [70]. A Laval nozzle was created with two diagonally opposite air channels, through which the airflow moved at supersonic speed (Mach number was 2). The details of calculating the characteristic dimensions of such a nozzle were described previously [70,71].

Table 1. Chemical composition of D16, AMg6 and A0 solid wires, wt.%.

	Fe	Si	Mn	Cr	Ti	Al	Cu	Mg	Zn
D16	0.22	0.41	0.85	0.05	0.12	93.11	4.14	1.05	0.05
AMg6	0.32	0.31	0.57	-	0.05	93.25	0.10	6.15	0.15
A0	0.21	0.18	-	-	-	99.6	0.01	-	-

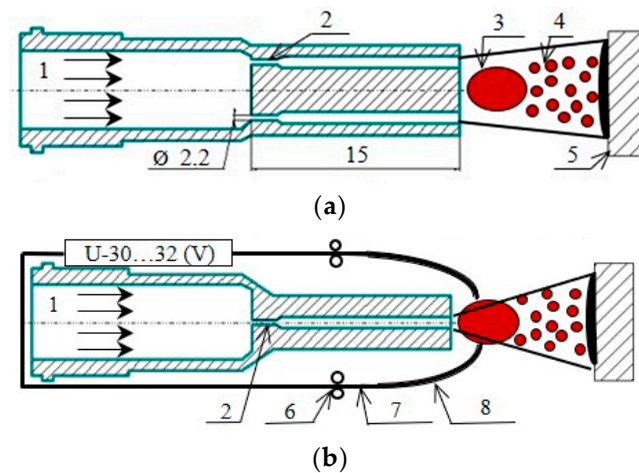


Figure 1. Schematic cross-section images of the metallizer nozzle for the formation of a supersonic spraying airflow (front view (a) and top view (b), respectively): 1—air flow, 2—critical section of a nozzle, 3—melt of electrode materials, 4—metal–air flow, 5—steel substrate with sprayed coating on the surface, 6—wires, 7—guides along which the electrodes are directed into the arc burning zone, 8—rollers for moving wire.

A TIMEZ-500 rectifier (Paton Welding Institute of the National Academy of Sciences of Ukraine, Kyiv, Ukraine) (voltage 30 V, current 150 A) was used to power the electric arc metallizer. The spraying distance was 120 mm. To increase the surface roughness of the substrate, the samples were previously treated by using a corundum with a diameter of 2–3 mm.

The tribological characteristics of the PEO layers were studied using an SMC-2 (Karpenko Physico-Mechanical Institute of the National Academy of Sciences of Ukraine, Lviv, Ukraine) tribo-tester (Figure 2), where the “disk-pad” friction pair was used. The change in the friction coefficient was determined at a sliding speed of 0.67 m/s and specific loads of 2–10 MPa. To achieve the specific loads of 2, 4, 6, 8 and 10 MPa used in our study, the pressing force for the tribopair elements was 330, 660, 990, 1320 and 1650 N, respectively. The contact area ratio during the friction tests was 0.125. The radial runout of the specimens did not exceed 0.02 mm.

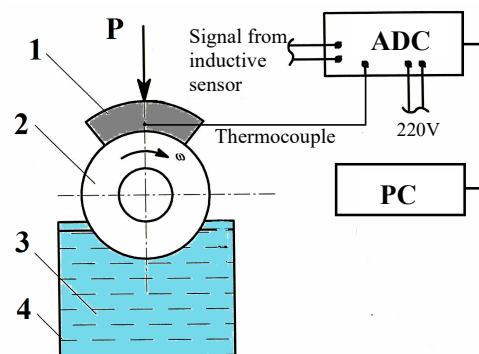


Figure 2. Scheme of the device for tribological investigations using the SMC-2 equipment: 1—counter body (segment), 2—disk specimen, 3—mineral oil; 4—bath for the oil. ADC—analogue-to-digital converter; PC—personal computer.

During the tests, the disk specimen (2), fixed onto the shaft of the equipment, was rotated at a given speed (300 min^{-1}) and partially immersed in a bath (3) with I-20 mineral oil. The friction torque was measured using a non-contact inductive sensor mounted onto the shaft of the equipment. The tribo-heating temperature of the friction pairs was measured using a chromel–alumel thermocouple mounted onto the counter body (1) at a distance of 0.5 mm from the friction zone. The electrical signals (in mV) from the inductive sensor and thermocouple, which characterize the friction torque (necessary to determine the friction coefficient) and the temperature of the specimen in the vicinity of the contact zone, were transmitted through an analog-to-digital converter and recorded in the computer memory. The recording step was 0.2 s. Based on these measurements, the dependencies of the change in the friction coefficient and temperature during testing were obtained.

In the friction tests, specimens in the form of disks with a diameter of $42 \pm 0.02 \text{ mm}$ were used. Specimens in the form of segments were used as the counter bodies. Their internal diameter corresponded to the external diameter of the disk, and the width of the friction track formed between the tribocontact elements was $10 \pm 0.1 \text{ mm}$. The disks and counter bodies were made of the D16 and AMg6 alloys, as well as from the same alloys but after surface hardening. To harden the surface of the alloys D16 and AMg6, either PEO treatment or complex treatment, consisting of two stages of hardening, was used. First, ASCs were applied to the working surfaces of the specimens intended for friction testing. These ASCs were deposited using electrodes made of the D16 alloy (hereafter referred to as ASC D16) or the AMg6 alloy (ASC AMg6). Then, oxide layers were synthesized on top of these ASCs on all the specimens using PEO processing. The PEO layers were formed in the cathodic–anodic mode with a pulsed current of 2 kA/m^2 at a ratio of the cathodic to the anodic currents $I_c/I_a = 1$ and a duration of synthesis of 120 min. To obtain PEO layers on the surface of the analyzed specimens, an electrolyte of the following composition was used: 3 g/l KOH + 2 g/l Na_2SiO_3 .

In addition, to rank the frictional characteristics of the hardened aluminum alloys, tribological tests were carried out using disks and counter bodies (segments) made from materials of different hardnesses. They were made from steel with galvanic chrome plating (hardness of 1050 HV), antifriction gray cast iron ACh-4 (hardness of 250 HV), steel ShKh15 (analog EN: 100Cr6 steel) with hardnesses of 780 HV and 330 HV, bronze BrC30 (analog CuPb30) with a hardness of 250 HV. Before testing, the surface of the specimens was polished. The roughness R_a of the specimens with PEO layers was 0.14–0.2 μm , and the roughness of the other materials was 0.06–0.08 μm .

Before friction testing, all the specimens were subjected to ultrasonic cleaning in ethyl alcohol, followed by drying in a thermostat at $80 \text{ }^\circ\text{C}$ for 20 min. After the friction tests with lubricant, the specimens were additionally kept in low-vacuum conditions (near 0.1 Pa) for 20 min (this is especially important for samples with PEO layers on ASCs) in order to eliminate residual lubricant from the pores of the coatings. This holding in a vacuum

was sufficient since repeated holding did not change the weight of the specimens. After being kept in vacuum, the specimens were cleaned in ethyl alcohol once more and dried before weighing.

Frictional wear was assessed according to the weight loss W of the specimens. For this purpose, all the specimens before and after the friction tests were weighed with an accuracy of 2×10^{-4} g using an electronic analytical balance of the KERN ABJ 220 4M type (Balingen, Germany). The wear value of each element in the analyzed friction pair was determined as the average value from at least three friction tests. The scatter of the data relative to the average value did not exceed 5%–7%.

X-ray micro-spectral analysis of the structure of the synthesized PEO layers was undertaken using an EVO 40 XVP (Carl Zeiss AG, Oberhofen, Germany) electron microscope with an INCA Energy 350 (Oxford Instruments, Wiesbaden, Germany) microanalysis system. A Bruker D8 DISCOVER (Bruker AXS, Frankfurt am Main, Germany) X-ray diffractometer with $\text{CuK}\alpha$ radiation was used for the phase analysis of the synthesized layers. The content of the phases in the surface layer was determined according to the X-ray diffraction patterns using the Rietveld method, using the FullProf software [72–74].

3. Results

3.1. Microstructure of the Analyzed PEO Layers

The typical microstructures in the cross-sections of the coatings are shown in Figures 3 and 4. In particular, Figure 3 shows the structure of a PEO layer synthesized on the surface of an ASC, previously deposited on the surface of the D16 alloy (substrate) using electrodes from the D16 alloy.

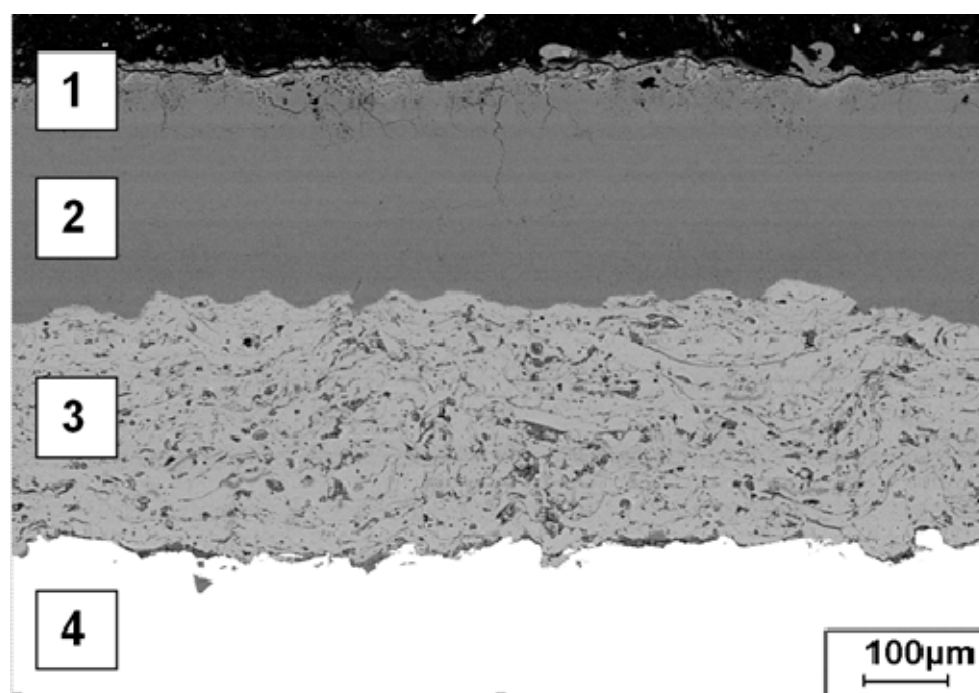


Figure 3. Typical microstructure in cross-section of specimen with PEO layer synthesized on ASC deposited using D16 wire: 1—technological PEO layer, 2—functional PEO layer, 3—remaining ASC, 4—D16 alloy substrate.

The microstructure of the PEO layers synthesized on the AMg6 and ASK AMg6 alloys is shown in Figure 4a,c,e. The micro-hardness of the PEO layers on the AMg6 alloy and the AMg6 ASC surface did not go beyond the range of 1400–1600 HV. The microstructure of the PEO layers synthesized on the D16 alloy and ASC D16 is presented in Figure 4b,d,f. Copper inclusions (bright visible light inclusions even at a low resolution) were found in

the structure of these PEO layers. The micro-hardness of the PEO layers on the alloy D16 and ASC D16 corresponded to the range of 1600–1800 HV.

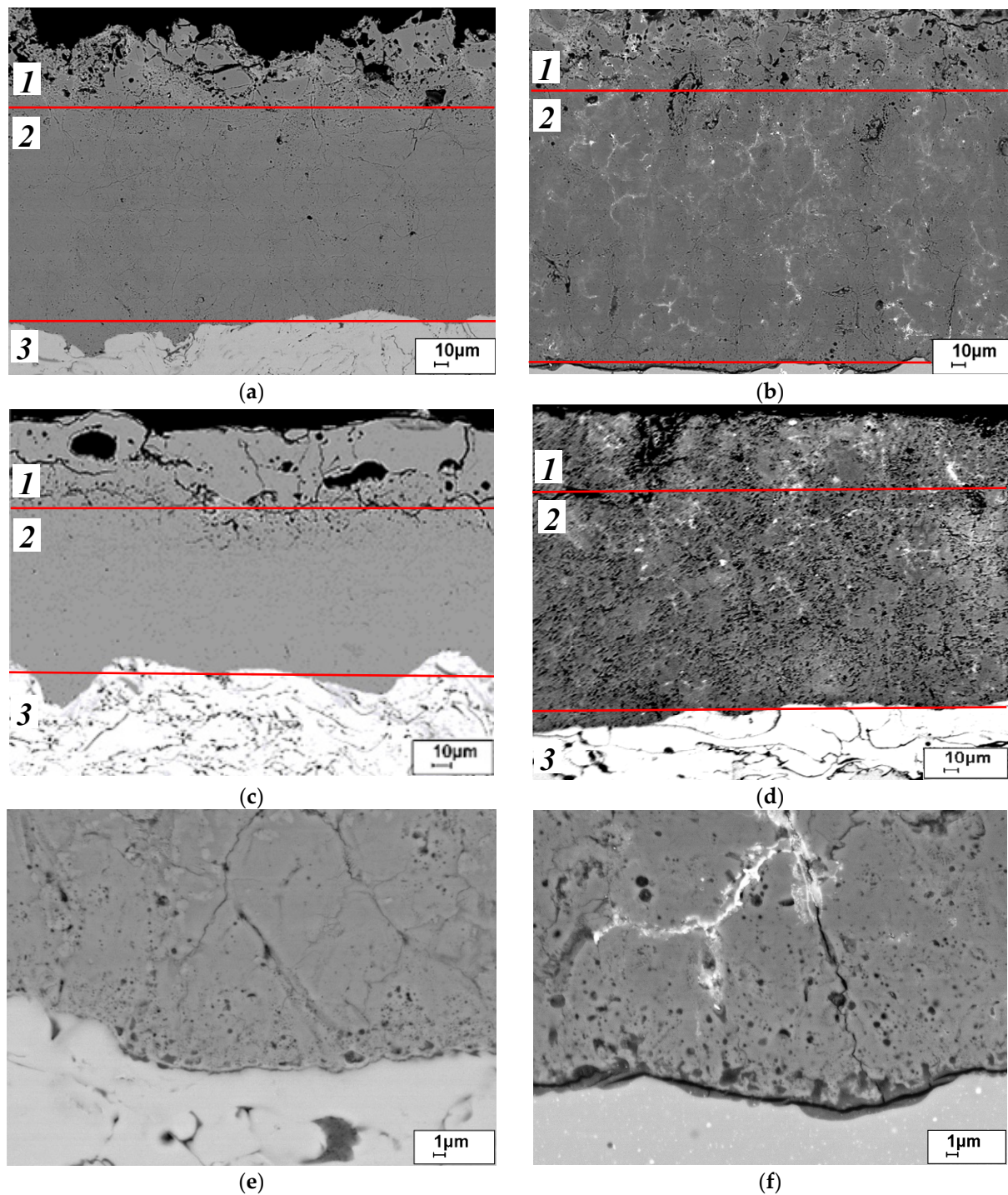


Figure 4. Microstructure of PEO synthesized on the surface of AMg6 (a) and D16 (b) alloys, as well as on the surface of ASC AMg6 (c,e) and ASC D16 (d,f), with sections of samples taken at low (a–d) and high (e,f) resolution. Red horizontal lines separate technological and functional zones of PEO layers from each other.

Higher-resolution photographs of the microstructure (Figure 4e,f) were obtained in the vicinity of the transition between the PEO layers (in the upper part of the photographs) and ASCs (in the lower part) formed on the AMg6 and D16 alloys using wires made from

the same alloys. At a high resolution, pores and microcracks appeared in the structure of the PEO layers (Figure 4e,f). Their appearance is due to the accelerated cooling of molten aluminum oxide during its synthesis due to the facilitated exchange of the electrolyte along the ASC pore chains. In the PEO layer on the ASC of the D16 alloy (Figure 4f), cracks were found filled with molten copper (more than 4 wt.% of which is contained in the D16 aluminum alloy, Table 1). This became possible due to the lower crystallization temperature of copper (1080 °C) compared to synthesized aluminum oxide (2050 °C).

3.2. Phase Composition of the PEO Layers on the Surfaces of the ASCs

Using X-ray phase analysis established that the main phases in the synthesized PEO layers are aluminum oxides with α and γ modifications. In some specimens, in addition to the two main phases (α -Al₂O₃ (JCPDS 46-1212) and γ -Al₂O₃ (JCPDS 47-1308)), a small amount of the metastable crystallized Al_{2.427}O_{3.64} phase (JCPDS 79-1559) was presented. In particular, the PEO layers synthesized on the D16 alloy contained 70% α -Al₂O₃ and 30% γ -Al₂O₃, while the content of these phases in the PEO layer synthesized on the surface of ASC D16 was 40 and 60%, respectively. The oxide–ceramic layers synthesized on the AMg6 alloy contained 30% α -Al₂O₃ and 70% γ -Al₂O₃, while in the synthesized PEO layer on ASC AMg6, their content was changed to 18 and 82%, respectively. The content of the phases in the surface layer was determined from the X-ray diffraction patterns using the Rietveld method, using the FullProf software.

The X-ray diffraction patterns of the PEO layers synthesized on the D16 and AMg6 alloys and on ASCs onto their surfaces are shown in Figures 5–8. The fitted lattice periods of the phases found in the PEO layers are given in Table 2.

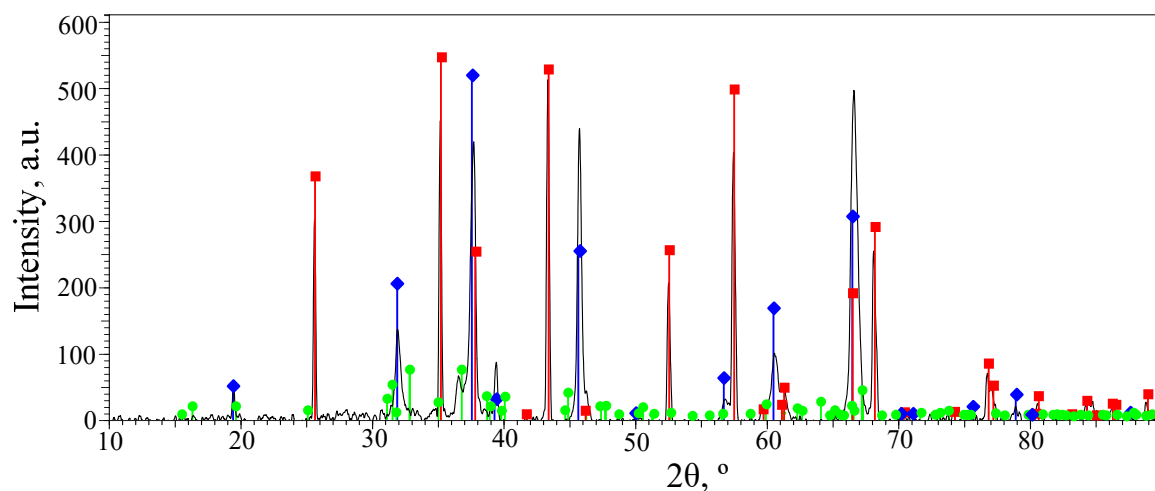


Figure 5. X-ray diffraction patterns of the PEO layer synthesized on D16 alloy: ■— α -Al₂O₃ with a hexagonal lattice; ◆— γ -Al₂O₃ with a cubic lattice; ●—Al_{2.427}O_{3.64}.

Table 2. Lattice periods for phases detected using X-ray phase analysis in PEO layers synthesized on the ASC D16 and ASC AMg16 surfaces.

Phase	SG	a	b	c
α -Al ₂ O ₃	R-3c	4.75980	4.75980	12.99240
γ -Al ₂ O ₃	Fd-3m	7.94800	7.94800	7.94800
Al _{2.427} O _{3.64}	C2/m	11.85400	2.90400	5.62200

The results of the X-ray phase analysis confirm that in some samples, in addition to the two main phases (α -Al₂O₃ and γ -Al₂O₃), traces of the metastable crystallized Al_{2.427}O_{3.64} phase are recorded.

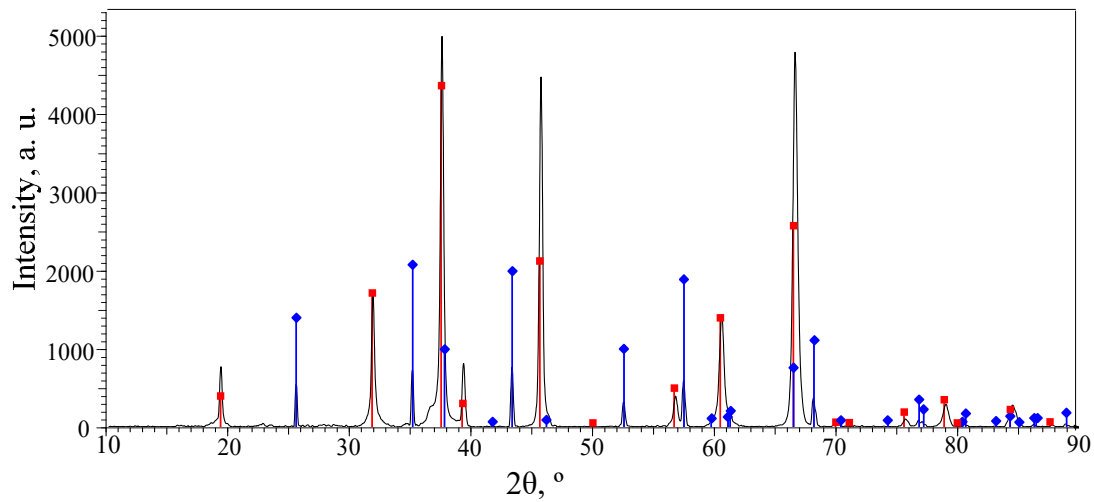


Figure 6. X-ray diffraction patterns of the PEO layer synthesized on the surface of ASC D16: ◆— α - Al_2O_3 with a hexagonal lattice; ■— γ - Al_2O_3 with a cubic lattice.

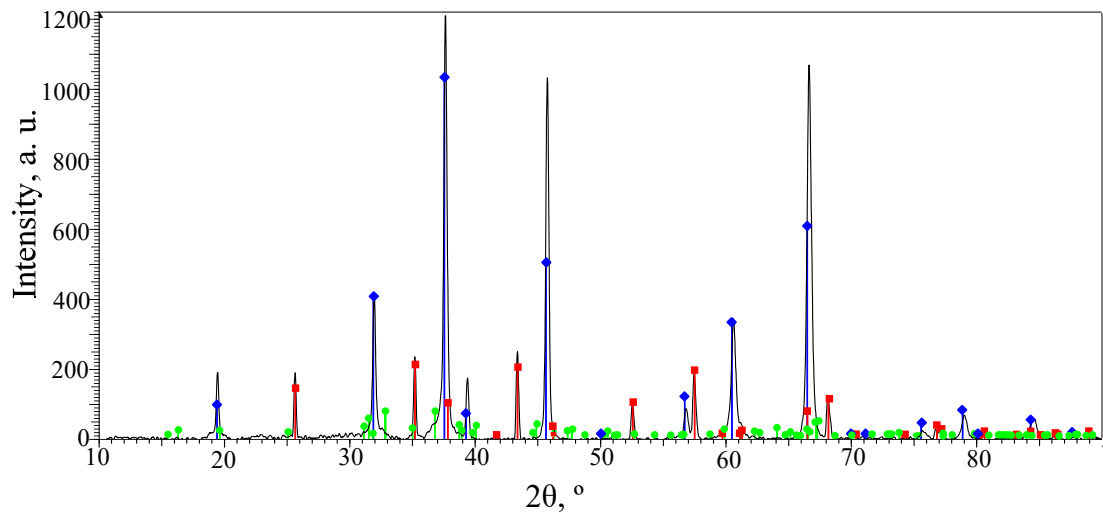


Figure 7. X-ray diffraction patterns of the PEO layer synthesized on AMg6 alloy: ■— α - Al_2O_3 with a hexagonal lattice; ◆— γ - Al_2O_3 with a cubic lattice; ●— $\text{Al}_{2.427}\text{O}_{3.64}$.

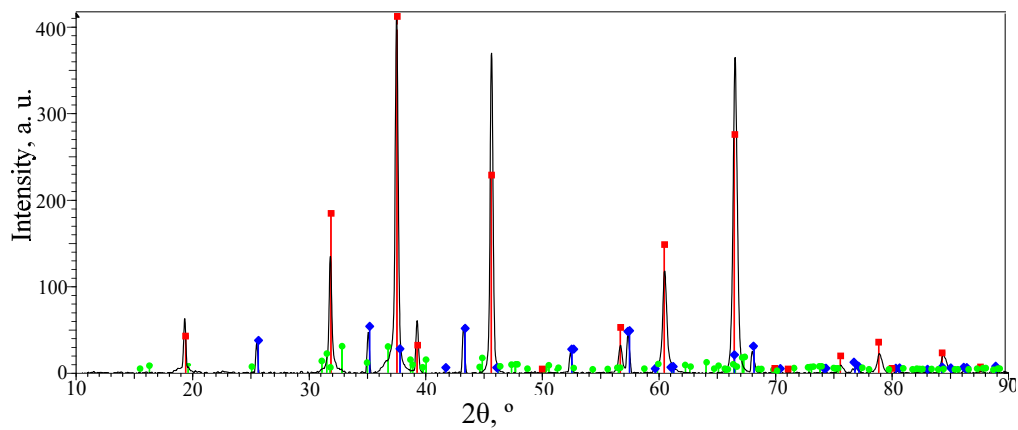


Figure 8. X-ray diffraction patterns of the PEO layer synthesized on the surface of ASC AMg6: ◆— α - Al_2O_3 with a hexagonal lattice; ■— γ - Al_2O_3 with a cubic lattice; ●— $\text{Al}_{2.427}\text{O}_{3.64}$.

3.3. Tribological Characteristics of the PEO Layers

According to the practice of operating many machines and structures, there are many combinations of materials used for the manufacture of tribocouple elements. The choice of the most effective friction pair is especially important for structurally and technologically complex machine elements. After all, the materials used for their manufacture, as a rule, cannot be changed. Therefore, it is necessary to select the most effective friction pair for a predetermined material with minimal wear of both elements. To this end, it is important to operate with information about the expected wear of the selected materials during their operation in pairs of direct and reverse friction (as a disk or a counter body). In subsequent parts of the paper, differences in the friction characteristics will be demonstrated both for a disk made of the D16 alloy with a PEO layer paired with different counter bodies and for a counter body made of the same D16 alloy with a PEO layer paired with different disks.

3.3.1. Wear Characteristics of a Disk Made of the D16 Alloy with a PEO Layer Paired with Various Counter Bodies (as Direct Friction Pairs)

The friction coefficients f and tribo-heating temperature T of the friction pairs were determined for 15 min during tests in I-20 mineral oil at a specific load of 4 MPa. Figure 9a makes it possible to compare the coefficients f for friction pairs between a disk made of D16 alloy with a PEO layer on its surface and counter bodies made of different materials. The lowest average value of the friction coefficient ($f = 0.01$) was found in the pair between a disk made of the aluminum alloy D16 with a PEO layer and a steel counter body hardened by galvanic chromium plating (Figure 9a, column 1). The f value increased by 0.013 upon frictional contact of the same disk with a counter body made of ShKh15 steel with a hardness of 780 HV (column 2). For the PEO layer on the D16 alloy disk paired with the same PEO layer on the counter body surface from the D16 alloy, the f value increased to 0.017 (columns 3). Whereas, during friction with a counter body made of cast iron, the friction coefficient increased to 0.02 (column 4). At the same time, during friction with the same disk, but with a counter body from ShKh15 steel with a hardness of 330 HV, it increased by more than an order of magnitude (column 5). For a friction pair between a PEO layer on the D16 alloy disk and a counter body made of bronze, the coefficient f increased to a maximum value of 0.2 (column 6).

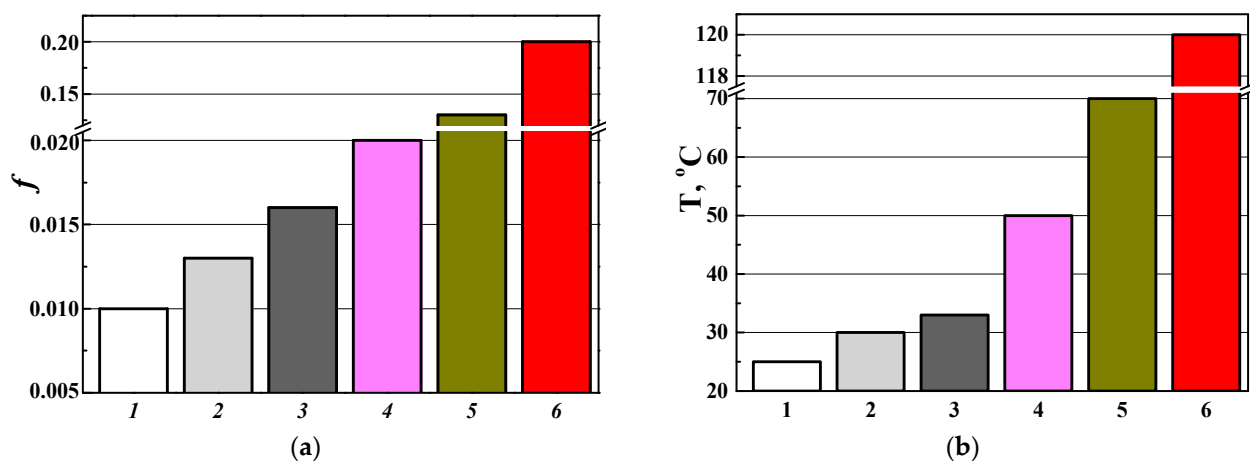


Figure 9. Average values of friction coefficients f (a) and temperature T (b) near the tribo-contact zone, determined after 15 min friction tests in I-20 mineral oil at a specific load $P = 4$ MPa, for a disk made of D16 alloy with PEO layer in a tribocouple with various counter bodies made of steel with galvanic chromium plating (1); steel ShKh15 with 780 HV (2); alloy D16 with PEO layer (3); cast iron ACh-4 (4); steel ShKh15 with hardness of 330 HV (5); bronze BrC30 (6).

The tribo-heating temperature near the contact zone of the analyzed friction pairs (a D16 alloy disk with a PEO layer in contact with various counter bodies) changed qual-

itatively, similarly to the friction coefficient (Figure 9b). The lowest temperature (about 25 °C) was recorded in the contact pair with the steel counter body with galvanic chromium plating (column 1). The temperature near the contact zone between the disk and the counter body made of steel with a hardness of 780 HV increased up to 30 °C (column 2), while it rose up to 33 and even 50 °C in contact with the counter bodies made of the D16 alloy with a PEO layer and made of cast iron (columns 3, 4). During the contact of the disk with the counter body made of steel with a hardness of 330 HV, the temperature increased up to 70 °C (column 5). The tribo-heating temperature reached a maximum value of 120 °C due to the contact of the D16 alloy disk with the PEO layer and the BrC30 bronze counter body (column 6).

Figure 10 makes it possible to compare the weight loss W of the various counter bodies (segments) after their friction tests with a disk made of the D16 alloy with a PEO layer under various specific loads P .

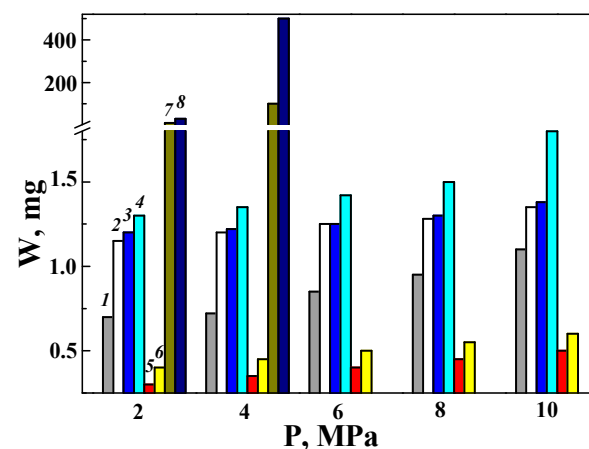


Figure 10. Average values of weight loss W depending on specific load P , determined for various counter bodies (segments) made of D16 (1) and AMg6 (2) alloys with PEO layers synthesized on their surfaces, as well as with PEO layers on the surface of ASC D16 (3) and ASC AMg6 (4) or made of steel with galvanic chromium plating (5), ShKh15 steel, heat-treated to a hardness of 780 HV (6) or 330 HV (7), as well as BrC30 bronze (8), obtained after 15 min of friction tests in I-20 mineral oil in a tribocouple with a disk made of D16 alloy with a PEO layer.

In such friction pairs, the weight loss of the counter body from the BrS-30 bronze was the greatest (column 8). The wear of the counter body made of steel with a hardness of 330 HV was slightly less than that of the bronze (column 7). Catastrophic wear of the bronze and the steel with a hardness of 330 HV occurred due to cutting with sharp protrusions on the PEO layer (due to the relatively high surface roughness), with the formation of a suspension of micron-sized chips in the oil. However, with an increase in the steel hardness to 780 HV, the weight loss of the counter body in the friction pair with a PEO layer on the D16 alloy decreased significantly (column 6). After the testing of the counter body made of steel with galvanic chromium plating paired with a disk from the D16 alloy with a PEO layer, its mass loss was the smallest (column 5).

The smallest mass loss of the counter bodies with PEO layers on various substrates was found for the D16 alloy with a PEO layer paired with a disk made of the same alloy after PEO treatment (columns 1, Figure 10). The wear of the other variants of counter bodies with synthesized PEO layers (PEO AMg16, PEO ASC D16, PEO ASC AMg16) was almost twice as large (columns 2–4) than in the case of both friction elements being made of PEO D16 (column 1). It was also noted that the weight losses of the counter bodies with PEO layers of options 2–4 remained practically unchanged with an increase in the specific load during friction. A slight increase in wear began to appear only at the maximum specific load of 10 MPa. Whereas, the wear of the counter body with PEO D16 paired with the

disk made of the D16 alloy with the same PEO layer increased more than 1.5 times with an increase in the specific stress to 10 MPa (columns 1).

Consequently, PEO treatment of the counter bodies made of both aluminum alloys and with ASCs on their surface significantly reduced the loss of their mass during friction when paired with the D16 alloy with a PEO layer (columns 1–4) compared to the low-strength steel and bronze (columns 7, 8). However, it increased their wear by 2–3 times compared to the accepted wear standards (high-strength steel and galvanically chrome-plated steel, columns 5, 6).

3.3.2. Wear Characteristics of a Counter Body Made of the D16 Alloy with a PEO Layer in Pairs with Various Disks (as Reverse Friction Pairs)

At low specific loads (2–6 MPa), the friction coefficient f changed insignificantly for all the analyzed friction pairs (Figure 11a). With an increase in the specific load of more than 6 MPa, the friction coefficient f for friction pairs (1), (2), (3) and (4) increased more significantly. The coefficient f reached the highest values for friction pairs (3) and (4). At the same time, this coefficient for friction pair (5) practically did not change with an increase in the specific load to 10 MPa. In our opinion, the high friction coefficients during tribo-contact of two surfaces with PEO layers (columns 3 and 4) are due to their high roughness after grinding ($R_a = 0.14–0.20$). Whereas, the roughness of the steel with a galvanic-chromium-plated surface after grinding was significantly less ($R_a = 0.08$). As a result, the friction coefficient of friction pair (5) remained low and did not depend on the value of the specific stress.

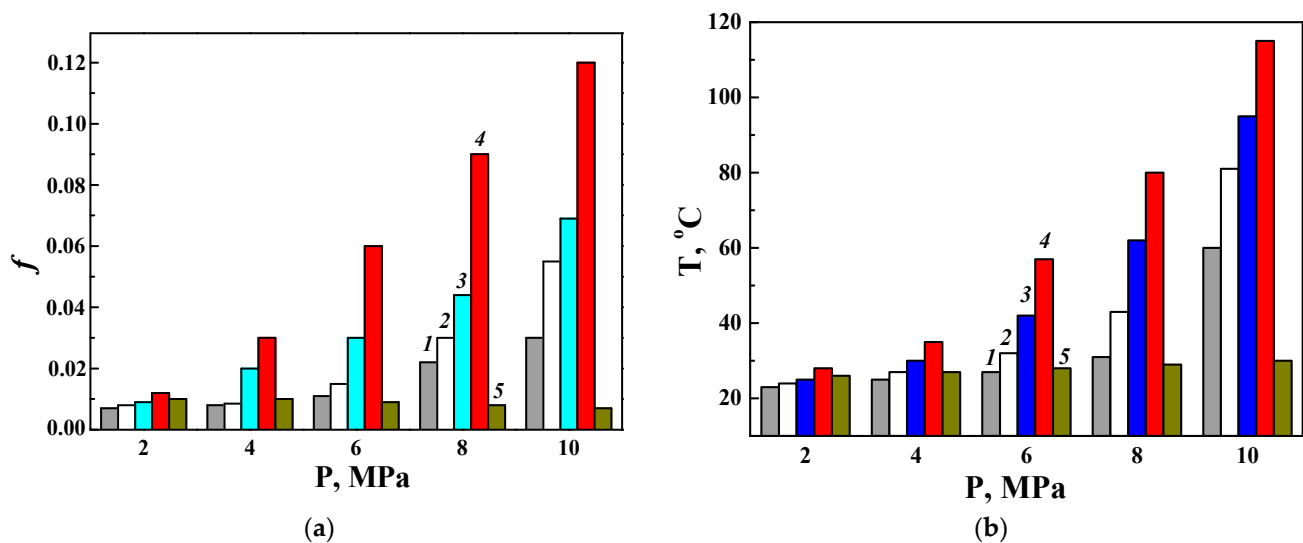


Figure 11. Average values of friction coefficients f (a) and temperature T near the tribo-contact zone (b), determined in I-20 mineral oil at different values of specific load P after 4 h of friction tests between a counter body (segment) made of D16 alloy, hardened with a PEO layer, and various disks made of alloys D16 (1), AMg6 (2), ASC D16 (3) and ASC AMg6 (4) with surface-hardened PEO layers, as well as steel with galvanic chromium plating (5).

The results show that during the 4 h tests, the temperature T in the vicinity of the contact zone of friction pair (5) did not depend on the specific load and did not exceed 27 °C (Figure 11b). At the same time, for all the other variants of friction pairs, the temperature clearly increased with increasing P . However, the nature of its change depends on the material, which was in contact with the counter body. The temperature in the contact zone in friction pairs (1) and (2) remained almost constant up to $P = 8$ MPa. Only at a specific load of 10 MPa did the temperature increase sharply by two times (for a pair where the counter body and disk were made of the alloy D16 with a PEO layer, column 1) and by more than 4 times (when the counter body and disk were made of different alloys D16 and

AMg6 with PEO layers on their surface, column 2). During the contact of the same counter body with the disks made of the D16 and AMg6 alloys with PEO layers synthesized on the ASC surfaces, the temperature in the zone of their contact increased gradually at a specific pressure of 4–6 MPa (columns 3 and 4). However, in a friction pair with a disk made of the AMg6 alloy with a PEO layer synthesized on the ASC surface, this occurred at lower specific load (column 4). In general, the changes in temperature in the contact zone of the analyzed tribocouples (Figure 11b) correlate well with the changes in the friction coefficients for them in mineral oil (Figure 11a). This confirmed the determining role of the friction coefficient between the elements of the friction pair on the temperature in the tribo-contact zone.

The data on the mass loss W of the disks made of various materials indicate that due to their frictional interaction with a counter body (segment) with PEO D16 in I-20 mineral oil, the W values for the steel disks with galvanic chromium plating were the smallest (Figure 12, column 5). At the same time, the weight loss of all four analyzed disks with PEO layers (columns 1–4) was 4–5 times greater than that of the steel disks with galvanic chromium plating, taken as the standard for comparison since they are the best option under friction conditions.

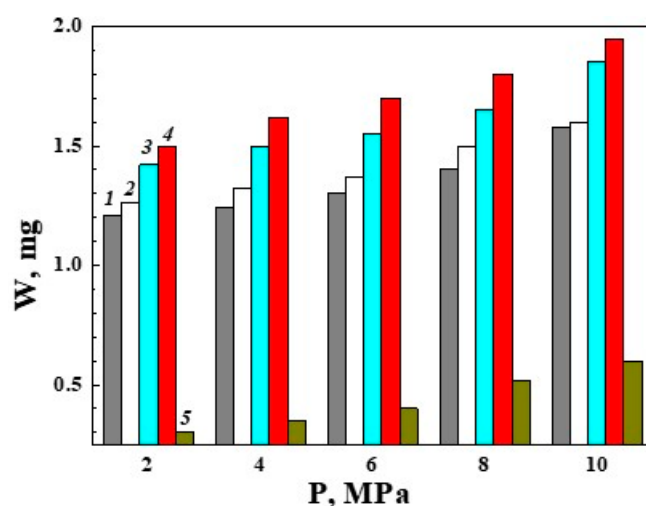


Figure 12. Average values of weight loss W depending on specific loads P , obtained for various disks made of D16 (1) and AMg6 (2) alloys with PEO layers synthesized on their surfaces, as well as with PEO layers on the surface of ASC D16 (3) and ASC AMg6 (4), or made of steel with galvanic chromium plating (5), after 4 h of friction tests in I-20 mineral oil in a tribocouple with a counter body made of D16 alloy with PEO layer.

In addition, it should be noted that, regardless of the specific load during the friction tests, the weight loss of the PEO layers synthesized on the disks made of the D16 and AMg6 alloys (columns 1, 2) was less than that of the PEO layers synthesized on the surfaces of ASC D16 and ASC AMg6 (columns 3, 4 respectively). The increase in the W values during the friction of the PEO layers synthesized on the ASCs, relative to those synthesized directly on the surface of both alloys, did not exceed 22%. The reason for this discrepancy may be the high porosity of the PEO layers synthesized on the ASCs. After all, an increase in the number of defects on the surface of the PEO layers will certainly intensify the wear of the disk during friction with the less defective surface of the counter body made of the D16 alloy with a PEO layer.

It is also noted that although the weight loss of the disks with all the analyzed PEO layers increases with an increasing specific load, the negative effect of the greater porosity of the PEO layers on the ASC surface did not increase more for the PEO layers directly on the aluminum alloys. This indicates good prospects for the use of a complex method

of hardening aluminum alloys. In particular, it will be useful for restoring the surfaces of expensive and structurally complex machine elements with traces of operational wear.

3.4. Reducing the Wear of the Disks with PEO Layers on ASCs Due to Modification of the Lubricating Medium

The method of X-ray spectral analysis revealed the segregation of copper particles on the friction surface of a disk (made of the D16 alloy with a PEO layer, synthesized on an ASC, sprayed with electrodes from the D16 alloy) paired with ShKh15 steel (Figure 13). X-ray phase analysis also confirmed the presence of copper and its compounds on the friction surface (Figure 14).

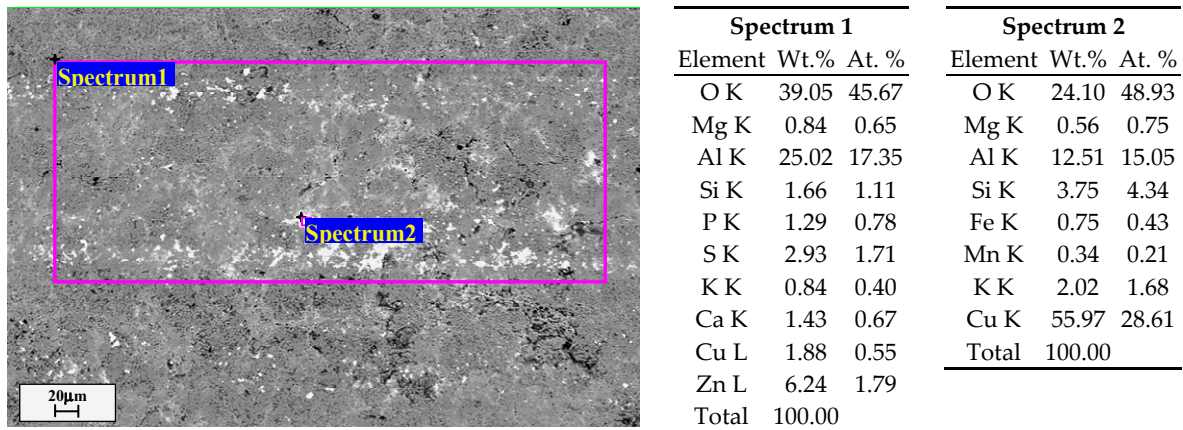


Figure 13. SEM topography with X-ray micro-spectral analysis of the friction surface of a disk (made of D16 alloy with a copper content of about 5 wt.% and with a PEO layer synthesized on ASC D16), obtained during tribo-contact at a specific load of 10 MPa with a counter body made of ShKh15 steel with a hardness of 780 MPa in 15W30 motor oil with the addition of 2.5 vol.% glycerin.

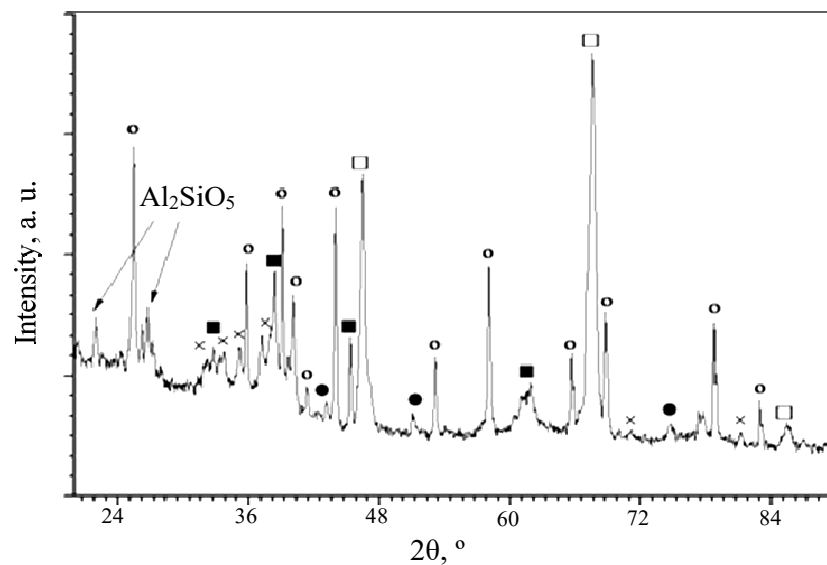


Figure 14. X-ray pattern obtained on the friction surface of a disk (made of D16 alloy with a copper content of more than 4 wt.% in its composition and with a PEO layer synthesized on ASC D16) during tribo-contact at a specific load of 10 MPa with a counter body made of ShKh15 steel with a hardness of 780 MPa in 15W30 motor oil with the addition of 2.5 vol.% glycerin: ○— γ - Al_2O_3 ; □— σ - Al_2O_3 ; ■— CuAl_2O_4 ; ●—Cu; ×—CuO.

It is known that during friction in an active medium (with glycerin additives), conditions may arise for selective transfer between tribocouple elements, which include copper or

a copper alloy and steel [75]. To test the possibility of realizing this effect, a series of friction tests were carried out in 15W30 motor oil and an oil–glycerin mixture (Figures 15 and 16).

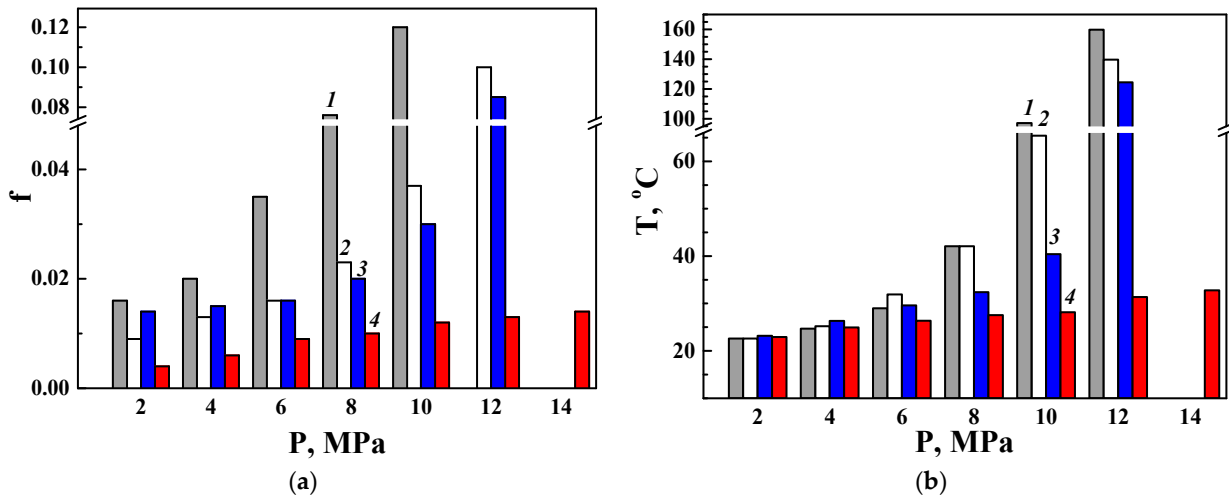


Figure 15. Change in the friction coefficient f (a) and tribo-heating temperature T (b) depending on the specific load P during friction tests of disks (made of D16 alloy with ASC sprayed using electrodes made of technical aluminum A0 (1, 2) or alloy D16 (3, 4), with subsequent synthesis of PEO layers on it) in tribo-contact with a counter body made of ShKh15 steel with a hardness of 780 HV in 15W30 motor oil (1, 3) and with the addition of 2.5 vol.% glycerin (2, 4).

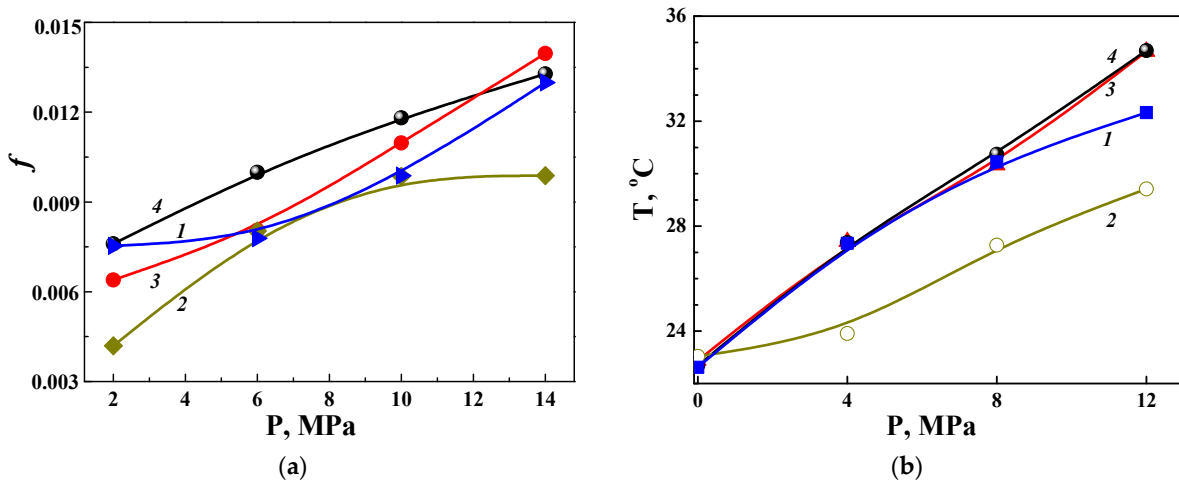


Figure 16. Friction coefficient f (a) and tribo-heating temperature T (b), determined at different specific loads P during friction tests of a disk (made of alloy D16 with ASC D16, on top of which a layer of PEO was synthesized) in tribo-contact with a counter body (steel ShKh15 with a hardness of 780 HV) in pure glycerin (1) and in motor oil 15W30 with the addition of 5 (2), 2.5 (3) and 1 (4) vol.% glycerin.

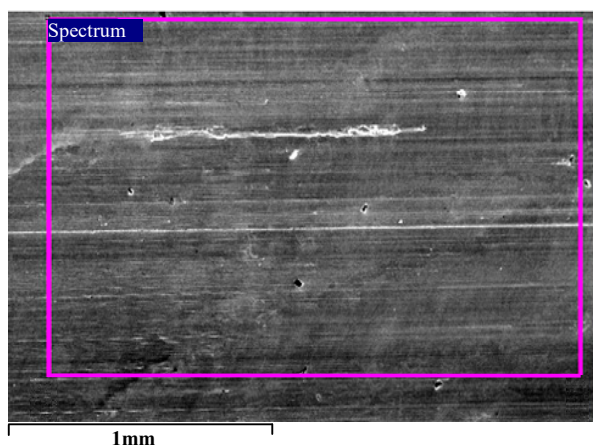
For this purpose, disks made of technical aluminum of grade A0 and the alloy D16 with PEO layers synthesized on an ASC, sprayed using electrodes made of A0 and D16, were tested in friction pairs with a counter body made of ShKh15 steel with a hardness of 780 MPa. It was established that the friction coefficient f between a disk made of the alloy D16 with a PEO layer synthesized on ASC D16 and a counter body made of steel ShKh15 is significantly reduced during friction tests in a mixture of 15W30 motor oil with 2.5 vol.% glycerin. The decrease in the coefficient f occurred over the entire studied range of changes in the specific load and ranged from 3.5 to 65 times at $P = 2$ and 12 MPa, respectively. The friction coefficient remained at a fairly low level (less than 0.015) up to a specific load of

14 MPa (Figure 15a, columns 4), and the tribo-heating temperature of the contacting pairs did not exceed 33 °C (Figure 15b, curve 4).

The decrease in the friction coefficient and the slowdown in the tribo-heating of the contact zone were less noticeable when tested in the same oil–glycerin mixture, using a disk with a PEO layer synthesized on an ASC surface using electrodes made of technical aluminum A0 (Figure 15, columns 2). In particular, by adding glycerin to the motor oil, the friction coefficient decreased by only 1.8 and 3.2 times at $P = 2$ and 10 MPa, respectively. At the same time, the temperature in the contact zones of this friction pair was also quite high and at $P = 12$ MPa reached 140 °C, which is only slightly lower than that achieved during friction in oil without the addition of glycerin (160 °C).

A comparison was also made of the tribological characteristics of one of the studied friction pairs (namely a disk made of alloy D16 with a PEO layer on ASC D16 in tribo-contact with a counter body made of hardened steel ShKh15) in pure glycerin and in a mixture with 15W30 motor oil in small quantities (5, 2.5 and 1 vol.%) of glycerin (Figure 16). It was established that even a small addition (1 vol.%) of glycerin to motor oil is enough to have almost the same effect on the friction characteristics in this composition as pure glycerin. We think that this is a consequence of the implementation of selective transfer in the analyzed friction pair under the influence of the addition of glycerin to the motor oil. After all, the disk is made of the D16 alloy, containing about 5 wt.% copper, and the PEO layer on its surface is synthesized on an ASC, also sprayed using electrodes made of the D16 alloy. In addition, segregation of the copper particles was found on its friction surface in motor oil with the addition of glycerin (Figures 13 and 14), which was not detected when tested in pure motor oil. Therefore, it could be that glycerol could promote the selective transfer of copper between the elements of the analyzed friction pair. However, with the addition of 5 vol.% glycerin to the motor oil, the friction coefficient and the tribo-heating temperature decreased to the lowest values (Figure 16a,b).

Upon completion of the friction tests, traces of copper deposits were also found on the surface of the steel counter body (Figure 17). This also indicates the possible implementation of the selective transfer of copper in a tribocouple of a disk (made of the D16 alloy with a layer of PEO synthesized on the ASC, sprayed using electrodes made of the D16 alloy) and a counter body made of ShKh15 steel in a motor oil environment with the addition of 2.5 vol.% glycerin.



Element	Wt.%	At.%
C K	7.04	25.96
Al K	0.31	0.51
Cr K	0.72	0.61
Fe K	91.69	72.75
Cu K	0.24	0.17
Total	100.00	

Figure 17. X-ray spectral mapping of the counter body surface (made of ShKh15 steel with a hardness of 780 HV) with secondary friction structures formed in a tribocouple with a disk (made of D16 alloy with a PEO layer synthesized on top of an ASC, sprayed using an electrode of D16 alloy) in a motor oil environment with a 2.5 vol.% of glycerin additive.

The presented research results, obtained during friction tests of a disk with a PEO layer on ASC D16 in a tribocouple with the hardened steel ShKh15, give grounds to assert that even a small amount of copper in the PEO layer is sufficient to implement selective

transfer of the copper between the elements of the friction pair. Moreover, this becomes possible even in the presence of a minimal amount of glycerin (starting from 1 vol.%) in the motor oil.

3.5. Discussion of the Possibilities of Using the Described Results

The most well-known publications have analyzed the tribological characteristics of friction pairs, for example, using a steel or ceramic ball with PEO layers synthesized on aluminum alloys [76–78]. These results are useful for justifying the choice of PEO modes and predicting wear resistance in air friction tests. However, they do not make it possible to predict the performance of elements processed using the PEO method when used in a friction pair with counter bodies made of traditional materials. The results described in the article make it possible to combine knowledge of and experience in using some of the most common methods of hardening the surfaces of aluminum alloys to form surface layers with new qualities and capabilities. The characteristics of the PEO layers synthesized both on homogeneous aluminum alloys and on ASCs on these alloys were analyzed in combination with counter bodies which are particularly common in the practice of operating various machines and mechanisms, such as bronze, cast iron and steels of varying hardness, as well as steel with galvanic chrome plating as a hardness standard.

There are different technologies which improve the tribological properties of friction surfaces under lubricated and non-lubricated conditions using aluminum and other materials [79–81], but in most cases, they are designed for use with flat and novel surfaces. The idea of combining two widely used surface treatment methods (PEO and ASC) arose regarding the problem of restoring expensive and heavily worn critical parts of complex geometries. Their wear resistance at the beginning of operation was ensured by plating their friction surfaces with galvanic chrome. PEO can compete with chromium plating in terms of hardness and wear resistance, but the limited thickness of the synthesized layers (up to 100 μm) does not allow the restoration of parts made of aluminum alloys with significant wear. Whereas, the arc spraying method makes it possible to restore the original dimensions of even heavily worn parts (the thickness of the coating can reach millimeters). However, ASCs do not have the necessary hardness and wear resistance to significantly extend the service life of the restored elements. Thus, the combination of these two methods has made it possible to significantly improve such functionally important properties of friction elements as hardness and wear resistance during friction without lubrication [43]. The high porosity of the ASCs had a negative effect on the efficiency of the PEO method. The use of supersonic ASCs in this study made it possible to reduce the porosity of the coatings (from 4–5 to 2.9 vol.%) and thereby enhance the positive effect of PEO. This expands the prospects for restoring complex parts operating in various friction pairs. The results obtained in the presented study clearly showed the advantages and disadvantages of the functional properties of various friction pairs combining traditionally used materials (cast iron, bronze and steel of different strength levels) with PEO layers. Therefore, these results are useful for justifying the choice of the optimal technology for the surface hardening of parts for specific operating conditions.

Moreover, adding even a small amount of glycerin to the working lubricant for the hardened elements can facilitate mass transfer between the friction elements. This is a new direction in searching for the resource capabilities of existing technologies in the field of surface engineering, with the expansion of their application to almost all the critical industries.

4. Conclusions

The performance of various variants of PEO layers synthesized on the surface of the hard aluminum alloys AMg6 and D16 and on ASCs deposited using electrodes made of the same alloys during tribocontact with high-hardness elements made of hardened or chrome-plated steel is substantiated.

The catastrophic wear of bronze and steel with a hardness of 330 HV during their friction with the PEO layers synthesized on the D16 alloy makes such tribocouples unsuitable for specific loads of more than 4 MPa. This is caused by the sharp protrusions on the surface of the very hard PEO layer (due to its relatively high roughness) that shear off the much softer layers of the bronze and steel, creating a suspension of micron chips in the oil.

It was established that during the frictional interaction of the disks (with PEO layers on the D16 alloy, as well as on the ASC D16 alloy) with the various counter bodies, the higher the micro-hardness of the counter body, the lower was its friction coefficient, tribo-heating temperature and weight loss. The minimum values of these characteristics were obtained in a friction pair between a disk with a PEO layer on D16 and a steel counter body with galvanic chromium plating, characterized by the maximum micro-hardness (1050 HV) among the analyzed counter bodies.

During the tribological interaction of a disk with a PEO layer on a D16 alloy, as well as on ASC D16 paired with a counter body made of ShKh15 steel (780 HV), in 15W30 motor oil with the addition of a small amount (up to 5 vol.%) of glycerin, the selective transfer of copper could be realized between the elements of the friction pair. Traces of copper were detected on the surfaces of both the steel counter body and the disk with a PEO layer. As a result, the friction coefficient decreased by an order of magnitude at high specific loads (up to 14 MPa).

Author Contributions: Conceptualization, V.H., M.S. and I.P.; methodology, V.H. and I.P.; validation, V.H. and K.Z.; formal analysis, I.P. and J.P.; investigation, V.H., and K.Z.; interpretation of results, M.S., V.H., I.P., O.S., J.P. and O.T.; resources, M.S. and I.P.; data curation, V.H., M.S., I.P., J.P., O.T. and O.S.; writing—original draft preparation, M.S., V.H., O.S. and K.Z.; discussion, M.S., I.P., O.S., J.P. and V.H.; writing—review and editing, M.S., O.S., R.R. and J.P.; visualization, V.H. and K.Z.; supervision, V.H. and M.S.; project administration, I.P. and M.S.; funding acquisition, M.S. All authors have read and agreed to the published version of the manuscript.

Funding: This research was carried out with financial support from the National Research Foundation of Ukraine within the framework of the project No. 2022. 01/0005 “The concept of restoring and extending exploitation resource of equipment of the most important branches of the national economy of Ukraine”.

Institutional Review Board Statement: Not applicable.

Informed Consent Statement: Not applicable.

Data Availability Statement: The data presented in this study are available upon request from the corresponding authors.

Conflicts of Interest: The authors declare no conflicts of interest.

References

1. Jiang, J.; Islam, M.A.; Xie, Y.; Stack, M.M. Some thoughts on modelling abrasion-corrosion: Wear by hard particles in corrosive environments. *J. Bio-Tribo-Corros.* **2024**, *10*, 12. [CrossRef]
2. Tartakovsky, E.D.; Goncharov, V.G.; Sapozhnikov, V.M. Analysis of the Effectiveness of Existing Methods of Repair 5D49 Diesel Engine Crankshafts. Available online: http://www.nbu.gov.ua/portal/natural/Znpudazt/2009_107/n107-71 (accessed on 25 January 2024).
3. Demin, A.Y.; Timofeeva, L.A.; Tymofeev, S.S.; Yagodinsky, E.S. Improved technologies at restoring crankshafts operational integrity for diesel vehicle destination. *East. Eur. J. Enterp. Technol.* **2014**, *1*, 60–64. [CrossRef]
4. Netchaev, G.; Baliczka, O. Increasing the industrial locomotives resource by improving technologies of the crankshaft engine rehabilitation. *Teka Comm. Mot. Energetics Agric.* **2012**, *12*, 176–181. Available online: <https://bibliotekanauki.pl/articles/792626> (accessed on 25 January 2024).
5. Lewis, R.; Dwyer-Joyce, R.S. Wear of diesel engine inlet valves and seat inserts. *Proc. Inst. Mech. Eng. Part D J. Automob. Eng.* **2002**, *216*, 205–216. [CrossRef]
6. Tomerlin, D. Repair welding of a rotating electrical machine’s broken shaft. *J. Weld. Cut.* **2019**, *18*, 198–203. Available online: <https://www.scribd.com/document/433680505/WEANDC-2019-3-198> (accessed on 25 January 2024).

7. Handbook of Reliability Prediction Procedures for Mechanical Equipment, Logistics Technology Support, Naval Surface Warfare Center (NSWC), Carderock Divizion, NSWC-11, West Bethesda, Maryland, May-2011, 20817–5700. Available online: <https://extapps.ksc.nasa.gov/Reliability/Documents/HandbookofMechanicalReliability.pdf> (accessed on 25 January 2024).
8. Survilienė, S.; Češūnienė, A.; Juškėnas, R.; Selskienė, A.; Bučinskienė, D.; Kalinauskas, P.; Juškevičius, K.; Jurevičiūtė, I. The use of trivalent chromium bath to obtain a solar selective black chromium coating. *Appl. Surface Sci.* **2014**, *305*, 492–497. [[CrossRef](#)]
9. Deflorian, F.; Rossi, S.; Fedrizzi, L.; Bonora, P.L. EIS study of organic coating on zinc surface pretreated with environmentally friendly products. *Prog. Org. Coat.* **2005**, *52*, 271–279. [[CrossRef](#)]
10. Bellezze, T.; Roventi, G.; Fratesi, R. Electrochemical study on the corrosion resistance of Cr III-based conversion layers on zinc coatings. *Surf. Coat. Technol.* **2002**, *155*, 221–230. [[CrossRef](#)]
11. Giovanardi, R.; Orlando, G. Chromium electrodeposition from Cr(III) aqueous solutions. *Surf. Coat. Technol.* **2011**, *205*, 3947–3955. [[CrossRef](#)]
12. Sheibani Aghdam, A.; Allahkaram, S.R.; Mahdavi, S. Corrosion and tribological behavior of Ni–Cr alloy coatings electrodeposited on low carbon steel in Cr (III)–Ni (II) bath. *Surf. Coat. Technol.* **2015**, *281*, 144–149. [[CrossRef](#)]
13. Rodríguez, R.J.; García, J.A.; Medrano, A.; Rico, M.; Sánchez, R.; Martínez, R.; Labrugère, C.; Lahaye, M.; Guette, A. Tribological behaviour of hard coatings deposited by arc-evaporation PVD. *Vacuum* **2002**, *67*, 559–566. [[CrossRef](#)]
14. Mutyala, K.C.; Ghanbari, E.; Doll, G.L. Effect of deposition method on tribological performance and corrosion resistance characteristics of Cr_xN coatings deposited by physical vapor deposition. *Thin Solid Films* **2017**, *636*, 232–239. [[CrossRef](#)]
15. Bembenek, M.; Makoviichuk, M.; Shatskyi, I.; Ropyak, L.; Pritula, I.; Gryn, L.; Belyakovskiy, V. Optical and mechanical properties of layered infrared interference filters. *Sensors* **2022**, *22*, 8105. [[CrossRef](#)] [[PubMed](#)]
16. Matthes, K.-J.; Honig, T.; Wielage, B.; Wank, A.; Podlesak, H.; Pokhmurska, H. Laserstrahl dispersieren von SiC in Aluminiumlegierungen zum partiellen Verschleißschutz. *Schweiss. Schneid.* **2006**, *58*, 119–122.
17. Zhai, W.; Zhu, Z.; Zhou, W.; Nai, S.M.L.; Wei, J. Selective laser melting of dispersed TiC particles strengthened 316L stainless steel. *Compos. Part B Eng.* **2020**, *199*, 108291. [[CrossRef](#)]
18. Kong, D.; Dong, C.; Ni, X.; Zhang, L.; Yao, J.; Man, C.; Cheng, X.; Xiao, K.; Li, X. Mechanical properties and corrosion behavior of selective laser melted 316L stainless steel after different heat treatment processes. *J. Mater. Sci. Technol.* **2019**, *35*, 1499–1507. [[CrossRef](#)]
19. Khakbiz, M.; Simchi, A.; Bagheri, R. Analysis of the rheological behavior and stability of 316L stainless steel–TiC powder injection molding feedstock. *Mater. Sci. Eng A.* **2005**, *407*, 105–113. [[CrossRef](#)]
20. Wank, A.; Schmengler, C.; Müller-Roden, K.; Beck, F.; Schläfer, T. Aptitude of different types of carbides for production of durable rough surfaces by laser dispersing. In Proceedings of the Thermal Spray International Thermal Spray, ITSC 2017, Düsseldorf, Germany, 7–9 June 2017; Paper No: itsc2017p0414. pp. 414–418, ISBN 9781510858220. [[CrossRef](#)]
21. Student, M.; Hvozdet'skyi, V.; Stupnyts'kyi, T.; Student, O.; Maruschak, P.; Prentkovskis, O.; Skačkauskas, P. Mechanical properties of arc coatings sprayed with cored wires with different charge compositions. *Coatings* **2022**, *12*, 925. [[CrossRef](#)]
22. Stupnyts'kyi, T.R.; Student, M.M.; Pokhmurs'ka, H.V.; Hvozdet's'kyi, V.M. Optimization of the chromium content of powder wires of the Fe–Cr–C and Fe–Cr–B systems according to the corrosion resistance of electric-arc coatings. *Mater. Sci.* **2016**, *52*, 165–172. [[CrossRef](#)]
23. Student, M.M.; Pokhmurs'ka, H.V.; Zadorozhna, K.R.; Veselivs'ka, H.H.; Hvozdet's'kyi, V.M.; Sirak, Y.Y. Corrosion Resistance of VC–FeCr and VC–FeCrCo Coatings Obtained by Supersonic Gas-Flame Spraying. *Mater. Sci.* **2019**, *54*, 535–541. [[CrossRef](#)]
24. Liu, N.; Liu, Q.; Li, Z.; Bai, Y.; Sun, Y.W.; Li, Z.D.; Bao, M.Y.; Zhan, H.; Guo, D.G.; Ma, Y.S. Tribological behavior of plasma-sprayed metal based solid self-lubricating coatings under heavy load. *Wear* **2021**, *486–487*, 204108. [[CrossRef](#)]
25. Zhao, X.; Li, S.; Hou, G.; An, Y.; Zhou, H.; Chen, J. Influence of doping graphite on microstructure and tribological properties of plasma sprayed 3Al₂O₃–2SiO₂ coating. *Tribol. Int.* **2016**, *101*, 168–177. [[CrossRef](#)]
26. Kumar, H.; Bhaduri, G.A.; Manikandan, S.G.K.; Kamaraj, M.; Shiva, S. Microstructural characterization and tribological properties of atmospheric plasma sprayed high entropy alloy coatings. *J. Therm. Spray Technol.* **2022**, *31*, 1956–1974. [[CrossRef](#)]
27. Pryszyzhnyuk, P.; Di Tommaso, D. The thermodynamic and mechanical properties of Earth-abundant metal ternary boride Mo₂(Fe,Mn)B₂ solid solutions for impact- and wear-resistant alloys. *Mater. Adv.* **2023**, *4*, 3822–3838. [[CrossRef](#)]
28. Hutsaylyuk, V.; Student, M.; Zadorozhna, K.; Student, O.; Veselivska, H.; Gvosdetskii, V.; Maruschak, P.; Pokhmurska, H. Improvement of wear resistance of aluminum alloy by HVOF method. *J. Mater. Res. Technol.* **2020**, *9*, 16367–16377. [[CrossRef](#)]
29. Fukumoto, M.; Wada, Y.; Umemoto, M.; Okane, I. Effect of connected pores on the corrosion behavior of plasma sprayed alumina coatings. *Surf. Coat. Technol.* **1989**, *39–40*, 711–720. [[CrossRef](#)]
30. Vlasiy, O.; Mazurenko, V.; Ropyak, L.; Rogal, O. Improving the aluminum drill pipes stability by optimizing the shape of protector thickening. *East.-Eur. J. Enterp. Technol.* **2017**, *1*, 25–31. [[CrossRef](#)]
31. Darband, G.B.; Aliofkhaezraei, M.; Hamghalam, P.; Valizade, N. Plasma-electrolytic oxidation of magnesium and its alloys: Mechanism, properties and applications. *J. Magnes. Alloys* **2017**, *5*, 74–132. [[CrossRef](#)]
32. Ropyak, L.; Shihab, T.; Velychkovych, A.; Bilinskyi, V.; Malinin, V.; Romaniv, M. Optimization of plasma electrolytic oxidation technological parameters of deformed aluminum alloy D16T in flowing electrolyte. *Ceramics* **2023**, *6*, 146–167. [[CrossRef](#)]
33. Ropyak, L.; Shihab, T.; Velychkovych, A.; Dubei, O.; Tutko, T.; Bilinskyi, V. Design of a two-layer Al–Al₂O₃ coating with an oxide layer formed by the plasma electrolytic oxidation of Al for the corrosion and wear protections of steel. *Prog. Phys. Met.* **2023**, *24*, 319–365. [[CrossRef](#)]

34. Shatskyi, I.; Makoviichuk, M.; Ropyak, L.; Velychkovych, A. Analytical model of deformation of a functionally graded ceramic coating under local load. *Ceramics* **2023**, *6*, 1879–1893. [[CrossRef](#)]
35. Nie, X.; Meletis, E.L.; Jiang, J.C.; Layland, A.; Yerokhin, A.L.; Matthews, A. Abrasive wear/corrosion properties and TEM analysis of Al₂O₃ coatings fabricated using plasma electrolysis. *Surf. Coat. Technol.* **2002**, *149*, 245–251. [[CrossRef](#)]
36. Wei, T.; Yan, F.; Tian, J. Characterisation and wear and corrosion-resistance of microarc oxidation ceramic coatings on aluminum alloy. *J. Alloys Compd.* **2005**, *389*, 169–176. [[CrossRef](#)]
37. Yerokhin, A.L.; Nie, X.; Leyland, A.; Matthews, A.; Dowey, S.J. Plasma electrolysis for surface engineering. *Surf. Coat. Technol.* **1999**, *122*, 73–93. [[CrossRef](#)]
38. Hutsaylyuk, V.; Student, M.; Dovhunyk, V.; Posuvailo, V.; Student, O.; Maruschak, P.; Koval'chuk, I. Effect of hydrogen on the wear resistance of steels upon contact with plasma electrolytic oxidation layers synthesized on aluminum alloys. *Metals* **2019**, *9*, 280. [[CrossRef](#)]
39. Simchen, F.; Sieber, M.; Kopp, A.; Lampke, T. Introduction to plasma electrolytic oxidation—An overview of the process and applications. *Coatings* **2020**, *10*, 628. [[CrossRef](#)]
40. Chumalo, H.V.; Posuvailo, V.M.; Kharchenko, E.V. Influence of the composition of electrolytes on the properties of plasma-electrolytic oxide coatings on light alloys. *Mater. Sci.* **2020**, *56*, 27–33. [[CrossRef](#)]
41. Posuvailo, V.M.; Klappiv, M.D.; Student, M.M.; Sirak, Y.Y.; Pokhmurska, H.V. Gibbs energy calculation of electrolytic plasma channel with inclusions of copper and copper oxide with Al-base. *Mater. Sci. Eng.* **2017**, *181*, 012045. [[CrossRef](#)]
42. Rodriguez, L.; Paris, J.-Y.; Denape, J.; Delbé, K. Micro-arcs oxidation layer formation on aluminium and coatings tribological properties—A review. *Coatings* **2023**, *13*, 373. [[CrossRef](#)]
43. Hutsaylyuk, V.; Student, M.; Posuvailo, V.; Student, O.; Sirak, Y.; Hvozdet's'kyi, V.; Maruschak, P.; Veselivska, H. The properties of oxide-ceramic layers with Cu and Ni inclusions synthesizing by PEO method on top of the gas-spraying coatings on aluminium alloys. *Vacuum* **2020**, *179*, 109514. [[CrossRef](#)]
44. Tu, C.; Chen, X.; Liu, C.; Li, D. Plasma electrolytic oxidation coatings of a 6061 Al alloy in an electrolyte with the addition of K₂ZrF₆. *Materials* **2023**, *16*, 4142. [[CrossRef](#)] [[PubMed](#)]
45. Zhang, Y.; Wang, Q.; Ye, R.; Ramachandran, C.S. Plasma electrolytic oxidation of cold spray kinetically metallized CNT-Al coating on AZ91-Mg alloy: Evaluation of mechanical and surficial characteristics. *J. Alloys Compd.* **2022**, *892*, 162094. [[CrossRef](#)]
46. Rao, Y.; Wang, Q.; Chen, J.; Ramachandran, C.S. Abrasion, sliding wear, corrosion, and cavitation erosion characteristics of a duplex coating formed on AZ31 Mg alloy by sequential application of cold spray and plasma electrolytic oxidation techniques. *Mater. Today Commun.* **2021**, *26*, 101978. [[CrossRef](#)]
47. Martin, J.; Akoda, K.; Ntomprougkidis, V.; Ferry, O.; Maizeray, A.; Bastien, A.; Brenot, P.; Ezo'o, G.; Henrion, G. Duplex surface treatment of metallic alloys combining cold-spray and plasma electrolytic oxidation technologies. *Surf. Coat. Technol.* **2020**, *392*, 125756. [[CrossRef](#)]
48. Martin, J.; Maizeray, A.; Tusch, C.; Da, S.; Marcos, G.; Czerwiec, T.; Henrion, G. A new strategy to prepare alumina-zirconia composite or multilayered coatings by combining cold-spray deposition and plasma electrolytic oxidation. *Mater. Today Commun.* **2023**, *36*, 106676. [[CrossRef](#)]
49. Champagne, V.; Helfritsch, D. The unique abilities of cold spray deposition. *Int. Mater. Rev.* **2016**, *61*, 437–455. [[CrossRef](#)]
50. Moridi, A.; Hassani-Gangaraj, S.M.; Guagliano, M.; Dao, M. Cold spray coating: Review of material systems and future perspectives. *Surf. Eng.* **2014**, *30*, 69–395. [[CrossRef](#)]
51. Ralls, A.; Gillespy, R.; Menezes, P.V.; Men, P.L. Unraveling electrochemical mechanisms in plasma electrolytic oxidation of cold spray additively manufactured stainless steel. *J. Mater. Eng. Perform.* **2023**, 1–19. [[CrossRef](#)]
52. Gu, W.; Shen, D.; Wang, Y.; Chen, G.; Feng, W.; Zhang, G.; Fan, S.; Liu, C.; Yang, S. Deposition of duplex Al₂O₃/aluminum coatings on steel using a combined technique of arc spraying and plasma electrolytic oxidation. *Appl. Surf. Sci.* **2006**, *252*, 2927–2932. [[CrossRef](#)]
53. Wu, Z.; Xia, Y.; Li, G.; Xu, F. Structure and mechanical properties of ceramic coatings fabricated by plasma electrolytic oxidation on aluminized steel. *Appl. Surf. Sci.* **2007**, *253*, 8398–8403. [[CrossRef](#)]
54. Student, M.M.; Pohrelyuk, I.M. Modification of the surfaces of aluminum and titanium alloys aimed at the improvement of their wear resistance and tribological characteristics. *Mater. Sci.* **2021**, *57*, 377–386. [[CrossRef](#)]
55. Dong, H.; Li, Q.; Xie, D.; Jiang, W.; Ding, H.; Wang, S.; An, L. Forming characteristics and mechanisms of micro-arc oxidation coatings on magnesium alloys based on different types of single electrolyte solutions. *Ceram. Int.* **2023**, *49*, 32271–32281. [[CrossRef](#)]
56. Habazaki, H.; Tsunekawa, S.; Tsuji, E.; Nakayama, T. Formation and characterization of wear-resistant PEO coatings formed on β-titanium alloy at different electrolyte temperatures. *Appl. Surf. Sci.* **2012**, *259*, 711–718. [[CrossRef](#)]
57. Kostelac, L.; Pezzato, L.; Colusso, E.; Natile, M.M.; Brunelli, K.; Dabalà, M. Black PEO coatings on titanium and titanium alloys produced at low current densities. *Appl. Sci.* **2023**, *13*, 12280. [[CrossRef](#)]
58. Ramazanova, Z.M.; Zamalitinova, M.G. Study of the properties of oxide coatings formed on titanium by plasma electrolytic oxidation method. *Eurasian Chem. Technol. J.* **2020**, *22*, 51–58. [[CrossRef](#)]
59. Arrabal, R.; Matykina, E.; Hashimoto, T.; Skeldon, P.; Thompson, G.E. Characterization of AC PEO coatings on magnesium alloys. *Surf. Coat. Technol.* **2009**, *203*, 2207–2220. [[CrossRef](#)]
60. Cui, S.; Han, J.; Du, Y.; Li, W. Corrosion resistance and wear resistance of plasma electrolytic oxidation coatings on metal matrix composites. *Surf. Coat. Technol.* **2007**, *201*, 5306–5309. [[CrossRef](#)]

61. Alshujery, M.K.; Al-Saadie, K.A.S. Corrosion inhibition of aluminum 6061 alloy by a micro arc oxidation modified with incorporated zinc oxide nanoparticles. *AIP Conf. Proc.* **2023**, *2830*, 020002. [[CrossRef](#)]
62. Lee, J.-M.; Kang, S.-B.; Han, J. Dry sliding wear of MAO-coated A356/20 vol.% SiCp composites in the temperature range 25–180 °C. *Wear* **2008**, *264*, 75–85. [[CrossRef](#)]
63. Lu, X.; Mohedano, M.; Blawert, C.; Matykina, E. Plasma electrolytic oxidation coatings with particle additions—A review. *Surf. Coat. Technol.* **2016**, *307*, 1165–1182. [[CrossRef](#)]
64. Xue, W.; Jin, Q.; Zhu, Q.; Hua, M.; Ma, Y. Anti-corrosion microarc oxidation coatings on SiC_p AZ31 magnesium matrix composite. *J. Alloys Compd.* **2009**, *482*, 208–212. [[CrossRef](#)]
65. Mingo, B.; Arrabal, R.; Mohedano, M.; Pardo, A. Corrosion and wear of PEO coated AZ91/SiC composites. *Surf. Coat. Technol.* **2017**, *309*, 1023–1032. [[CrossRef](#)]
66. Matykina, E.; Arrabal, R.; Skeldon, P.; Thompson, G.E. Investigation of the growth processes of coatings formed by AC plasma electrolytic oxidation of aluminium. *Electrochim. Acta* **2009**, *54*, 6767–6778. [[CrossRef](#)]
67. Dehnavi, V.; Shoesmith, D.W.; Li, B.; Yari, M.; Yang, X.; Rohani, S. Corrosion properties of plasma electrolytic oxidation coatings on an aluminium alloy—The effect of the PEO process stage. *Mater. Chem. Phys.* **2015**, *161*, 49–58. [[CrossRef](#)]
68. Mingo, B.; Arrabal, R.; Mohedano, M.; Llamazares, Y.; Matykina, E.; Yerokhin, A.; Pardo, A. Influence of sealing post-treatments on the corrosion resistance of PEO coated AZ91 magnesium alloy. *Appl. Surf. Sci.* **2018**, *433*, 653–667. [[CrossRef](#)]
69. Egorkin, V.S.; Gnedenkov, S.V.; Sinebryukhov, S.L.; Vyaliy, I.E.; Gnedenkov, A.S.; Chizhikov, R.G. Increasing thickness and protective properties of PEO-coatings on aluminum alloy. *Surf. Coat. Technol.* **2018**, *334*, 29–42. [[CrossRef](#)]
70. Student, M.; Gvozdetzky, V.; Student, O.; Prentkovskis, O.; Maruschak, P.; Olenyuk, O.; Titova, L. The effect of increasing the air flow pressure on the properties of coatings during the arc spraying of cored wires. *J. Mech. Eng.-Stroj. Časopis* **2019**, *69*, 133–146. [[CrossRef](#)]
71. Gurvich, L.V.; Veyts, I.V.; Medvedev, V.A.; Khachkuruzov, G.A.; Yungman, V.S.; Bergman, G.A.; Baybuz, V.F.; Iorish, V.S.; Yurkov, G.N.; Gorbov, S.I.; et al. *Thermodynamic Properties of Individual Substances*; Hemisphere Publishing Corp.: New York, NY, USA, 1989; Volume 1, Part 2; 340p.
72. Gualtieri, A.F.; Gatta, G.D.; Arletti, R.; Artioli, G.; Ballirano, P.; Cruciani, G.; Guagliardi, A.; Malferrari, D.; Masciocchi, N.; Scardi, P. Quantitative phase analysis using the Rietveld method: Towards a procedure for checking the reliability and quality of the results. *Period. Miner.* **2019**, *88*, 147–151. [[CrossRef](#)]
73. Altomare, A.; Cuocci, C.; Gatta, G.D.; Moliterni, A.; Rizzi, R. Methods of crystallography: Powder X-ray diffraction. *EMU Notes Mineral.* **2017**, *19*, 79–138. [[CrossRef](#)]
74. Bish, D.L.; Howard, S.A. Quantitative phase analysis using the Rietveld method. *J. Appl. Crystallogr.* **1988**, *21*, 86–91. [[CrossRef](#)]
75. Ilie, F. Diffusion and mass transfer mechanisms during frictional selective transfer. *Int. J. Heat Mass Transf.* **2018**, *116*, 1260–1265. [[CrossRef](#)]
76. Chen, Q.; Lei, M.; Chen, Y.; Deng, Y.; Chen, M.-A. Preparation of a thick sponge-like structured amorphous silica ceramic coating on 6061 aluminum alloy by plasma electrolytic oxidation in TEOS solution. *Ceram. Int.* **2023**, *49*, 32679–32693. [[CrossRef](#)]
77. Yang, X.; Chen, L.; Jin, X.; Du, J.; Xue, W. Influence of temperature on tribological properties of microarc oxidation coating on 7075 aluminium alloy at 25 °C–300 °C. *Ceram. Int.* **2019**, *45*, 12312–12318. [[CrossRef](#)]
78. Shirani, A.; Joy, T.; Rogov, A.; Lin, M.; Yerokhin, A.; Mogonye, J.-E.; Korenyi-Both, A.; Aouadi, S.M.; Voevodin, A.A.; Berman, D. PEO-Chameleon as a potential protective coating on cast aluminum alloys for high-temperature applications. *Surf. Coat. Technol.* **2020**, *397*, 126016. [[CrossRef](#)]
79. Kirik, G.V.; Gaponova, O.P.; Tarelnyk, V.B.; Myslyvchenko, O.M.; Antoszewski, B. Quality Analysis of Aluminized Surface Layers Produced by Electrospark Deposition. *Powder Metall. Met. Ceram.* **2018**, *56*, 688–696. [[CrossRef](#)]
80. Zhang, F.; Chen, J.; Yan, S.; Yu, G.; He, J.; Yin, F. Plasma spraying Ti–Al–C based composite coatings from Ti/Al/graphite agglomerates: Synthesis, characterization and reaction mechanism. *Vacuum* **2022**, *200*, 111036. [[CrossRef](#)]
81. Rukanskis, M.; Padgurskas, J.; Mihailov, V.; Rukuiža, R.; Žunda, A.; Baltakys, K.; Tuckute, S. Investigation of the Lubricated Tribo-System of Modified Electrospark Coatings. *Coatings* **2023**, *13*, 825. [[CrossRef](#)]

Disclaimer/Publisher’s Note: The statements, opinions and data contained in all publications are solely those of the individual author(s) and contributor(s) and not of MDPI and/or the editor(s). MDPI and/or the editor(s) disclaim responsibility for any injury to people or property resulting from any ideas, methods, instructions or products referred to in the content.